Published September 22, 2014

Mastl is required for timely activation of APC/C in meiosis I and Cdk1 reactivation in meiosis II

Deepak Adhikari,[1] M. Kasim Diril,[2] Kiran Busayavalasa,[1] Sanjiv Risal,[1] Shoma Nakagawa,[3] Rebecca Lindkvist,[1] Yan Shen,[1] Vincenzo Coppola,[4] Lino Tessarollo,[4] Nobuaki R. Kudo,[3] Philipp Kaldis,[2,5] and Kui Liu[1]

[1]Department of Chemistry and Molecular Biology, University of Gothenburg, S-405 30 Gothenburg, Sweden
[2]Institute of Molecular and Cell Biology, A*STAR, Singapore 138673, Republic of Singapore
[3]Institute of Reproductive and Developmental Biology, Department of Surgery and Cancer, Hammersmith Hospital, Imperial College London, London W12 0NN, England, UK
[4]National Cancer Institute, Mouse Cancer Genetics Program, National Cancer Institute–Frederick, Frederick, MD 21702
[5]Department of Biochemistry, National University of Singapore, Singapore 117599, Republic of Singapore

In mitosis, the Greatwall kinase (called microtubule-associated serine/threonine kinase like [Mastl] in mammals) is essential for prometaphase entry or progression by suppressing protein phosphatase 2A (PP2A) activity. PP2A suppression in turn leads to high levels of Cdk1 substrate phosphorylation. We have used a mouse model with an oocyte-specific deletion of *Mastl* to show that *Mastl*-null oocytes resume meiosis I and reach metaphase I normally but that the onset and completion of anaphase I are delayed. Moreover, after the completion of meiosis I, *Mastl*-null oocytes failed to enter meiosis II (MII) because they reassembled a nuclear structure containing decondensed chromatin. Our results show that Mastl is required for the timely activation of anaphase-promoting complex/cyclosome to allow meiosis I exit and for the rapid rise of Cdk1 activity that is needed for the entry into MII in mouse oocytes.

Introduction

Meiotic maturation of mammalian oocytes consists of two consecutive M phases, meiosis I and meiosis II (MII), without an intervening S phase. As in mitosis, entry into both of the meiotic M phases is driven by the activity of Cdk1 in association with cyclin B (Jones, 2004). The resumption of oocyte meiosis I, as characterized by germinal vesicle (GV) breakdown (GVBD), is considered to be equivalent to the mitotic G2/M transition (Eppig et al., 2004; Jones, 2004).

After GVBD in mouse oocytes, Cdk1 activity increases gradually during the lengthy prometaphase of meiosis I (Polanski et al., 1998; Kitajima et al., 2011; Davydenko et al., 2013). Once metaphase I is reached, a transient decrease in Cdk1 activity leads to the extrusion of the first polar body (PB1) as a result of the degradation of cyclin B1. This degradation is mediated by the ubiquitin ligase anaphase-promoting complex/cyclosome (APC/C) that is loaded with its targeting subunit Cdc20. In mitosis, APC/C activity is regulated by the modulation of Cdc20 through phosphorylation, degradation, or the direct binding to inhibitory proteins (Pesin and Orr-Weaver, 2008). The regulation of APC/C activity in mammalian meiosis remains poorly understood, but recent findings show that mitogen-activated protein kinase and Cdk1 are involved in the regulation of APC/C during meiosis I progression in mouse oocytes (Nabti et al., 2014). Once anaphase I is completed, Cdk1 activity is up-regulated rapidly, and this is essential for entry into MII. The elevated Cdk1 activity peaks at metaphase II (MetII) and remains high until fertilization (Kubiak et al., 1992).

Recent studies have indicated that an increase in Cdk1 activity alone is not sufficient for mitotic progression and that a simultaneous suppression of antagonizing protein phosphatase activity is also required (Virshup and Kaldis, 2010). Greatwall (Gwl) kinase or its mammalian orthologue microtubule-associated serine/threonine kinase like (Mastl) is the key regulator that suppresses protein phosphatase activity and thus plays an important role in mitotic progression in all model systems tested so far, including *Drosophila melanogaster*, *Xenopus laevis* egg

S. Risal and S. Nakagawa contributed equally to this paper.

Correspondence to Philipp Kaldis: kaldis@imcb.a-star.edu.sg; or Kui Liu: kui.liu@gu.se

V. Coppola's present address is Dept. of Molecular Virology, Immunology, and Medical Genetics, The Ohio State University, Columbus, OH 43210.

Abbreviations used in this paper: APC/C, anaphase-promoting complex/cyclosome; dbcAMP, dibutyryl-cAMP; Ensa, endosulfine α; ES, embryonic stem; GV, germinal vesicle; GVBD, GV breakdown; Gwl, Greatwall; hCG, human chorionic gonadotropin; Mastl, microtubule-associated serine/threonine kinase like; MetII, metaphase II; MII, meiosis II; OA, okadaic acid; PB1, first polar body; PBE, PB1 extrusion; PMSG, pregnant mare serum gonadotropin; SAC, spindle assembly checkpoint.

Supplemental Material can be found at:
http://jcb.rupress.org/content/suppl/2014/09/22/jcb.201406033.DC1.html

The Rockefeller University Press $30.00
J. Cell Biol. Vol. 206 No. 7 843–853
www.jcb.org/cgi/doi/10.1083/jcb.201406033

Published September 22, 2014

extracts, and mammalian cell lines (Yu et al., 2004, 2006; Archambault et al., 2007; Burgess et al., 2010; Voets and Wolthuis, 2010; Glover, 2012; Lorca and Castro, 2012; Álvarez-Fernández et al., 2013; Wang et al., 2013). In addition, Gwl function has also been shown to be important for the entry into meiosis I in *Xenopus* oocytes (Dupré et al., 2013), the entry and progression of meiosis I in *Drosophila* (Kim et al., 2012; Von Stetina et al., 2008), and in in vitro–studied porcine oocytes (Li et al., 2013). Gwl is also required for chromosome segregation during meiosis I in starfish oocytes (Okumura et al., 2014) and for the temporal order of anaphase and cytokinesis at the end of mitotic M phase (Cundell et al., 2013).

In *Xenopus* egg extracts, Gwl promotes mitotic entry and progression by phosphorylating endosulfine α (Ensa) and cAMP-regulated phosphoprotein 19 (Arpp19), which in their phosphorylated states bind and inhibit protein phosphatase 2A (PP2A)–B55 and prevent dephosphorylation of Cdk1 substrates (Gharbi-Ayachi et al., 2010; Mochida et al., 2010; Virshup and Kaldis, 2010). This pathway is conserved and plays an important role in regulating both mitosis and meiosis in *Drosophila* (Von Stetina et al., 2008; Rangone et al., 2011; Wang et al., 2011). It was also reported in *Xenopus* oocytes that protein kinase A maintains the meiotic arrest at prophase I by phosphorylating Arpp19 at serine 109 (Dupré et al., 2013, 2014).

To understand the functions of Mastl in the meiotic divisions of mammalian oocytes, we generated a mutant mouse model in which *Mastl* was deleted specifically in oocytes. Our results demonstrate that although Mastl is not required for the resumption of meiosis and progression to metaphase I, it plays an important role in the timely activation of APC/C at the end of meiosis I. Moreover, Mastl is indispensable for the rapid Cdk1 reactivation that is essential for MII entry.

Results and discussion

Infertility of Oo*Mastl*$^{-/-}$ mice and delayed onset of anaphase I in oocytes

We first investigated the expression pattern of the Mastl protein during oocyte maturation and transition into embryos. As shown in Fig. S1 A, Mastl was expressed in mouse oocytes throughout the maturation process and in early embryos. Notably, Mastl protein levels were elevated in the oocytes at MetII, and Mastl exhibited slower migration (Fig. S1 A) as a result of its phosphorylation status in prometaphase I and MetII oocytes (Fig. S1 B). Immunofluorescence microscopy indicated that Mastl was localized in the GV before meiotic resumption but was found throughout the ooplasm after GVBD and in MetII oocytes (Fig. S1 C).

To determine the functions of Mastl during oocyte maturation, we generated a mouse model in which exon 4 of the *Mastl* gene is flanked by two *loxP* sequences (*Mastl*^{FLOX}; Fig. S1, D and E). We crossed these mice with *Zona pellucida 3* (*Zp3*)–*Cre* mice (de Vries et al., 2000) to specifically inactivate the *Mastl* gene in mouse oocytes during the early stages of oocyte growth (Fig. S1 F). The resulting mice (*Mastl*$^{FLOX/FLOX}$;*Zp3-Cre*) are referred to as Oo*Mastl*$^{-/-}$ mice, and *Mastl*$^{FLOX/FLOX}$ mice are labeled as Oo*Mastl*$^{+/+}$. Immunoblotting confirmed that the Mastl protein was already completely absent in GV-stage Oo*Mastl*$^{-/-}$ oocytes (Fig. S1 G).

Oo*Mastl*$^{-/-}$ females were found to be infertile (Fig. S2 A), but the ovarian development and ovulation of Oo*Mastl*$^{-/-}$ females were normal (not depicted). The requirement of Mastl/Gwl during the entry into meiosis I in *Xenopus* oocytes (Dupré et al., 2013), the entry and progression of meiosis I in *Drosophila* (Von Stetina et al., 2008; Kim et al., 2012) and porcine oocytes (Li et al., 2013), and the progression of meiosis in starfish oocytes (Okumura et al., 2014) led us to assume that the *Mastl*-deficient oocytes would fail to progress through meiosis I. However, we found that in vitro–cultured Oo*Mastl*$^{-/-}$ oocytes underwent GVBD with kinetics and efficiencies that were indistinguishable from those of Oo*Mastl*$^{+/+}$ oocytes (Fig. 1 A). Oo*Mastl*$^{-/-}$ oocytes progressed to metaphase I with chromosome condensation and spindle formation comparable with those of Oo*Mastl*$^{+/+}$ oocytes (Fig. 1 B, Fig. S2 B, and Videos 1 and 2). The spindles migrated toward the cortex normally in *Mastl*-deficient oocytes (Fig. 2 D, right; and Video 2). These results suggest that Mastl has no essential role during meiotic resumption or prometaphase I progression in mouse oocytes.

In Oo*Mastl*$^{+/+}$ oocytes, PB1 extrusion (PBE), an event marking the completion of meiosis I, had occurred by 12 h after GVBD ($n = 60$) in vitro. In contrast, only ∼60% of Oo*Mastl*$^{-/-}$ oocytes extruded PB1 at 16 h after GVBD ($n = 57$; Fig. 1 C). Live cell imaging confirmed normal metaphase I entry but delayed PBE in Oo*Mastl*$^{-/-}$ oocytes (Fig. 2 D, right; and Video 2). However, it is worth noting that the in vivo PBE rate of ovulated Oo*Mastl*$^{-/-}$ oocytes (97.03%, $n = 236$) was comparable with Oo*Mastl*$^{+/+}$ oocytes (97.77%, $n = 90$) when collected at 16 h after human chorionic gonadotropin (hCG) treatment (Fig. 1 D). Thus, Oo*Mastl*$^{-/-}$ oocytes are capable of completing meiosis I after a delay. It is possible that oocytes complete meiosis I faster under more optimal in vivo conditions than those in more challenging in vitro cultures. Thus the differences in the timing of completing meiosis I between the control and mutant oocytes might be missed in vivo.

To study whether the delayed PBE rate in Oo*Mastl*$^{-/-}$ oocytes is caused by a delayed activation of APC/C during meiosis I, we monitored the timing of endogenous securin degradation, which mirrors APC/C activity during oocyte maturation (McGuinness et al., 2009). We found that in Oo*Mastl*$^{+/+}$ oocytes, securin levels had already decreased at 9 h after GVBD (Fig. 1 E). In contrast, the securin level in Oo*Mastl*$^{-/-}$ oocytes still remained high at 9 h after GVBD but was decreased at 14 h after GVBD, suggesting a delayed degradation of securin in Oo*Mastl*$^{-/-}$ oocytes (Fig. 1 E). Thus, Mastl is required for the timely activation of APC/C that is needed for the completion of meiosis I in mouse oocytes.

We checked whether the suppressed APC/C activity in the Oo*Mastl*$^{-/-}$ oocytes was caused by spindle assembly checkpoint (SAC) activation because of possible subtle defects in spindle and/or chromosome alignment. As an indicator of the SAC status, we examined the localization of the checkpoint protein Mad2, which binds to unattached kinetochores but is released upon the formation of stable microtubule–kinetochore attachments at metaphase I (Wassmann et al., 2003). As shown

Published September 22, 2014

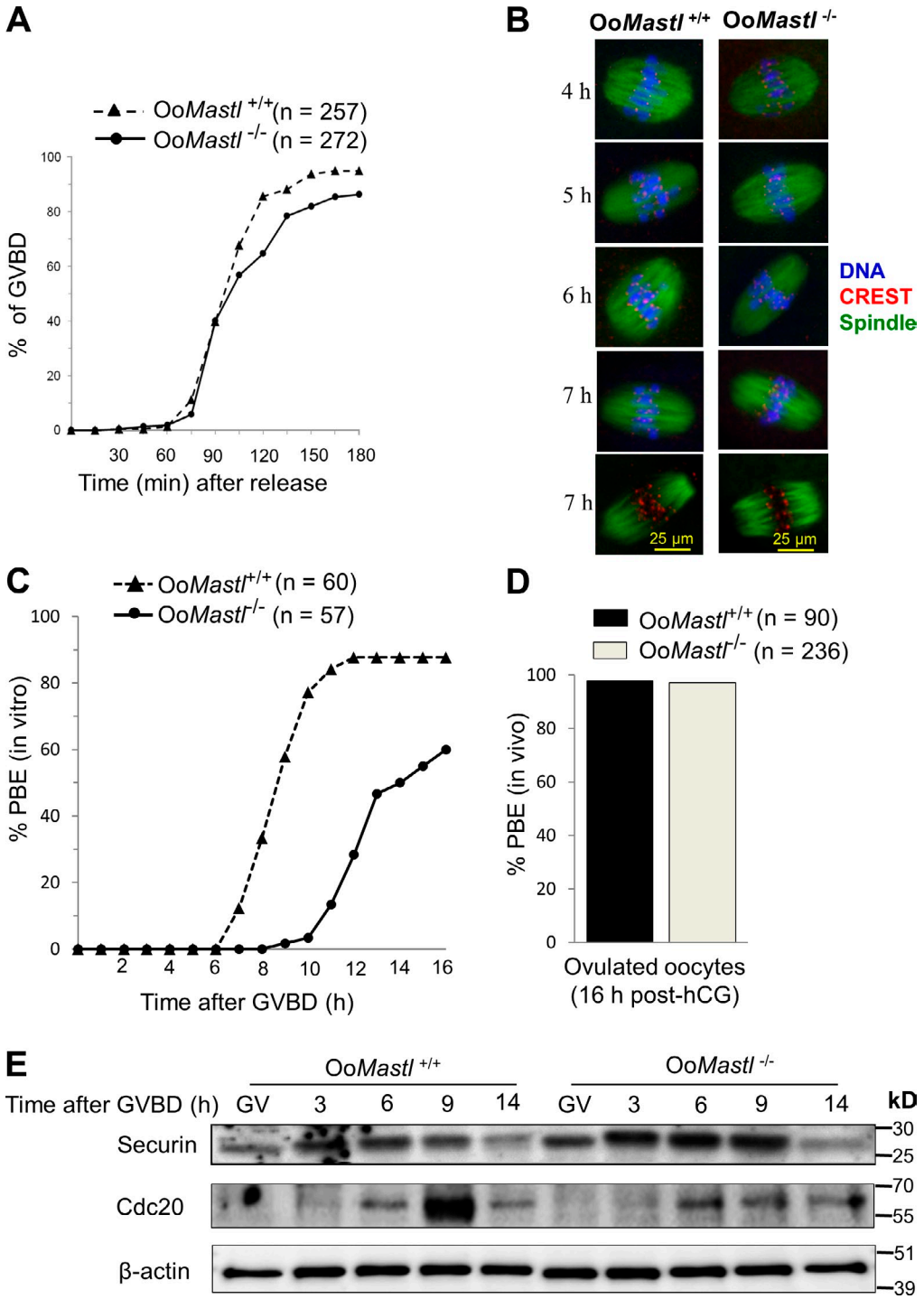

Figure 1. **Meiotic maturation of Oo*Mastl*$^{-/-}$ oocytes.** (A) Comparison of the kinetics of GVBD after release from dbcAMP. The total numbers of oocytes used (n) are indicated. (B) Representative images of immunostaining for DNA, CREST, and spindle showing normal progression to metaphase I in Oo*Mastl*$^{-/-}$ oocytes. Oocytes were cultured for the indicated periods after GVBD and were fixed. 30 oocytes were analyzed for each time point. (C) Kinetics of PBE. Oocytes that had undergone GVBD within 2 h after release into dbcAMP-free M16 medium were selected (at time = 0) and cultured further. PBE was scored at 1-h intervals. The numbers of oocytes examined are indicated (n). (D) Comparable PBE rates of the ovulated oocytes collected at 16 h after hCG. The numbers of oocytes used (n) are shown. All of the experiments were repeated at least three times, and representative results are shown. (E) Western blots showing the timing of securin degradation and Cdc20 level during oocyte maturation. Lysate from 100 oocytes was loaded in each lane. The levels of β-actin were used as a control. The same β-actin panel is presented again in Fig. 3 B, which shows the expression of other proteins of interest in the same cell lysates.

in Fig. S2 C, we detected Mad2 staining in virtually every kinetochore in both control and mutant oocytes at prometaphase I (3 h after GVBD). Subsequently, Mad2 was completely dissociated from kinetochores of Oo*Mastl*$^{-/-}$ oocytes at metaphase I (7 h after GVBD) when stable kinetochore–microtubule attachments were established, and this was similar to the Oo*Mastl*$^{+/+}$ oocytes (Fig. S2 C). Therefore, we propose that the activation of SAC in *Mastl*-null oocytes occurs normally as in the wild-type oocytes.

Published September 22, 2014

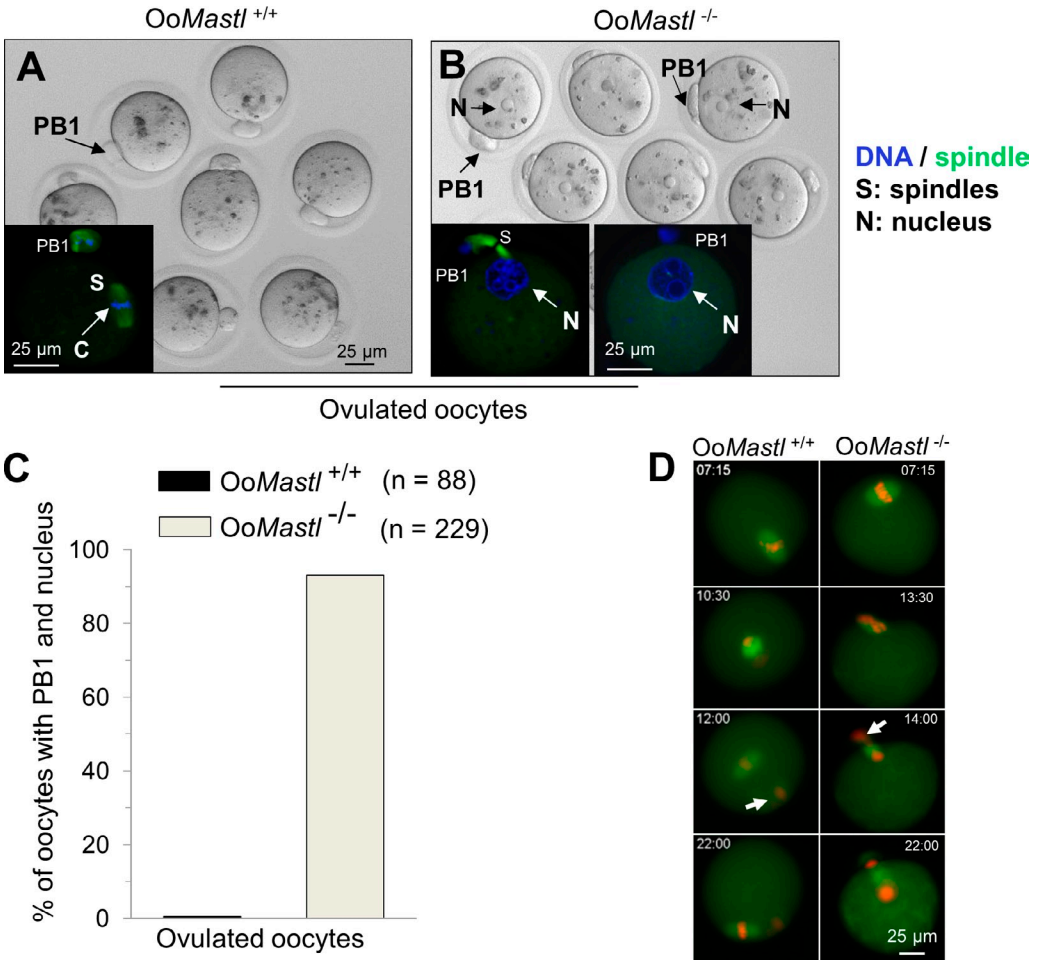

Figure 2. **Failure of Oo*Mastl*$^{-/-}$ oocytes to enter MII after PBE.** (A) Oo*Mastl*$^{+/+}$ oocytes formed MetII spindles with condensed chromosomes (C) after PBE. (B) Oo*Mastl*$^{-/-}$ oocytes extruded PB1s but formed nuclei with decondensed chromatin. In some oocytes (left inset), the nuclei had already formed, whereas the residual central spindle microtubules remained between the chromatin in the PB1 and the nucleus. 50 oocytes from each group were analyzed, and representative images are shown. (C) The percentages of oocytes with both a PB1 and a nucleus. For A–C, ovulated (16 h after hCG) oocytes were used. (D) Representative still images from Videos 1 and 2. Timestamps indicate hours and minutes after release from IBMX. H2B-mCherry (red fluorescence) shows the DNA, and Map7-EGFP (green fluorescence) labels the spindle microtubules. Arrows indicate the positions of PB1s.

In addition, we found that in contrast to Oo*Mastl*$^{+/+}$ oocytes in which the level of Cdc20 was increased at 9 h after GVBD when the activity of APC/C is elevated, the level of Cdc20 in Oo*Mastl*$^{-/-}$ oocytes remained low at this time (Fig. 1 E). A previous study has shown that PBE is delayed when the amount of Cdc20 protein is limited in mouse oocytes (Jin et al., 2010), and this appears to be a similar phenomenon to what we observed in the *Mastl*-null oocytes. Thus, we hypothesize that Mastl might regulate APC/C activity directly during meiosis I by regulating the levels of Cdc20. Because the regulation of the multisubunit complex of APC/C in mouse oocytes is far from being completely understood, however, the possibility of other regulatory mechanisms being involved cannot be discounted.

Oo*Mastl*$^{-/-}$ oocytes cannot enter MII

Although Oo*Mastl*$^{-/-}$ oocytes completed meiosis I in vivo with normal cytokinesis (Fig. 1 D) and extruded morphologically normal PB1s (Fig. 2 B), confocal microscopy revealed that after PBE, Oo*Mastl*$^{-/-}$ oocytes contained distinct nuclei with decondensed chromatin in both the oocytes and the PB1 (Fig. 2, B ["PB1" and "N" in insets] and C). This was in sharp contrast to the typical bipolar MetII spindles and aligned chromosomes seen in the Oo*Mastl*$^{+/+}$ oocytes (Fig. 2 A, inset). In 33% ($n = 229$) of the Oo*Mastl*$^{-/-}$ oocytes, residual central spindle microtubules were still visible between the decondensed chromatin in the PB1 and the nucleus (Fig. 2 B, left inset, ovulated oocytes 16 h after hCG). Moreover, live cell imaging revealed that after PBE, Oo*Mastl*$^{-/-}$ oocytes decondensed their chromatin and did not reform the MetII bipolar spindle (Fig. 2 D and Video 2). These results suggest that Mastl is essential for MII entry. The Oo*Mastl*$^{-/-}$ oocytes subsequently entered S phase after PBE (Fig. S2 D), and within 24 h of in vitro culture, most of the Oo*Mastl*$^{-/-}$ oocytes were cleaved into two cells and subsequently degenerated (not depicted).

Oo*Mastl*$^{-/-}$ oocytes up-regulate Cdk1 activity normally during prometaphase I but fail to increase Cdk1 activity for the entry into MII

To investigate the activity of Cdk1 in Oo*Mastl*$^{-/-}$ oocytes throughout the maturation process, we performed in vitro kinase

Published September 22, 2014

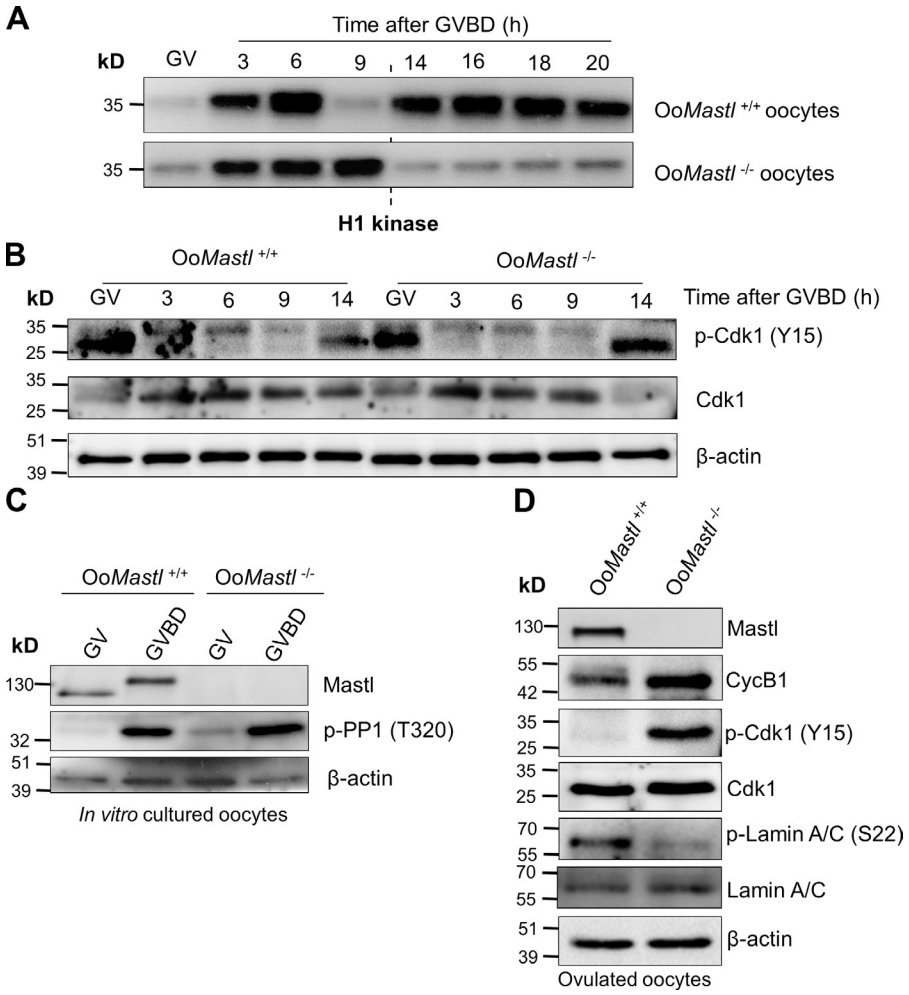

Figure 3. **Cdk1 activity during oocyte maturation.** (A) Comparable Cdk1 activities during prometaphase I (3 h) and metaphase I (6 h) but delayed reduction in Cdk1 activity in Oo*Mastl*$^{-/-}$ oocytes (9 h). Cdk1 activity cannot be increased after PBE (14 h) in Oo*Mastl*$^{-/-}$ oocytes (bottom right). (B) Western blots showing the dynamics of p-Cdk1 (Y15) during oocyte maturation. Lysate from 100 oocytes was loaded in each lane. The levels of β-actin and Cdk1 were used as controls. The same β-actin panel is presented in Fig. 1 E, which shows the expression of other proteins of interest in the same cell lysates. (C) Comparable PP1 phosphorylation (indicating inhibition) at GVBD in Oo*Mastl*$^{-/-}$ and Oo*Mastl*$^{+/+}$ oocytes. (D) Expression of Mastl, cyclin B1, p-Cdk1 (Y15), Cdk1, phospho–lamin A/C (S22), and lamin A/C in ovulated oocytes. β-Actin was used as the loading control. Lysate from 100 oocytes was loaded in each lane.

assays. From the GV stage to prometaphase I (3 h after GVBD) and metaphase I (6 h after GVBD) stages, both Oo*Mastl*$^{+/+}$ and Oo*Mastl*$^{-/-}$ oocytes displayed similar increases in Cdk1 activity (Fig. 3 A, left of the dashed line). Consistent with the similar levels of Cdk1 activity, both Oo*Mastl*$^{+/+}$ and Oo*Mastl*$^{-/-}$ oocytes displayed similar levels of inhibitory phosphorylation on Cdk1 (Y15) at the GV stage and subsequent dephosphorylation after GVBD (Fig. 3 B). We also found that during prometaphase I the endogenous Cdk1 substrate, PP1, was phosphorylated on residue T320 to a similar degree in both Oo*Mastl*$^{+/+}$ and Oo*Mastl*$^{-/-}$ oocytes (Fig. 3 C). These results demonstrate that *Mastl*-deficient oocytes are capable of phosphorylating Cdk1 substrates through normal up-regulation of Cdk1 activity; thus, the progression through prometaphase I in the Oo*Mastl*$^{-/-}$ oocytes appears to be normal.

We measured PP2A activity in the oocytes (as described in Materials and methods) and found that the PP2A activities in both Oo*Mastl*$^{+/+}$ and Oo*Mastl*$^{-/-}$ oocytes were comparable at the GV and GVBD stages (Fig. S3 A). Thus, our results suggest that mouse oocytes progress through prometaphase I without suppressing PP2A activity and, therefore, that Mastl regulation of PP2A does not play a major role during prometaphase I.

Nevertheless, Cdk1 activity in Oo*Mastl*$^{+/+}$ oocytes sharply decreased at the time of anaphase I onset (9 h after GVBD), which is caused by cyclin B1 degradation mediated by APC/C as has been shown previously (Madgwick et al., 2006; Jin et al., 2010). In contrast, the Cdk1 activity in Oo*Mastl*$^{-/-}$ oocytes remained high at this point (Fig. 3 A), which is likely caused by low APC/C activity (as shown in Fig. 1 E) in Oo*Mastl*$^{-/-}$ oocytes. This result suggests that Mastl plays an essential role in triggering the activation of APC/C that is required for the down-regulation of Cdk1 activity and that this mediates the timely onset of anaphase I in mouse oocytes.

The activation of Cdk1 that is required for the entry into MII and the following arrest at MetII (Kubiak et al., 1992) was observed in Oo*Mastl*$^{+/+}$ oocytes at 14 h after GVBD and after further culture for up to 20 h (Fig. 3 A, top right). However, the Cdk1 activity in Oo*Mastl*$^{-/-}$ oocytes failed to increase after PBE and remained at low levels throughout the extended culture period (Fig. 3 A, bottom right). This indicates that in the absence of Mastl, the rapid elevation in Cdk1 activity, which is needed for MII entry, was completely inhibited. As another indicator of Cdk1 activity, the level of phosphorylation of lamin A/C, an endogenous Cdk1 substrate (Peter et al., 1990; Haas and Jost, 1993), was decreased after PBE in Oo*Mastl*$^{-/-}$ oocytes (Fig. 3 D, ovulated oocytes), which might directly trigger the reformation of the nuclear membrane in the mutant oocytes (Fig. 2 B).

Published September 22, 2014

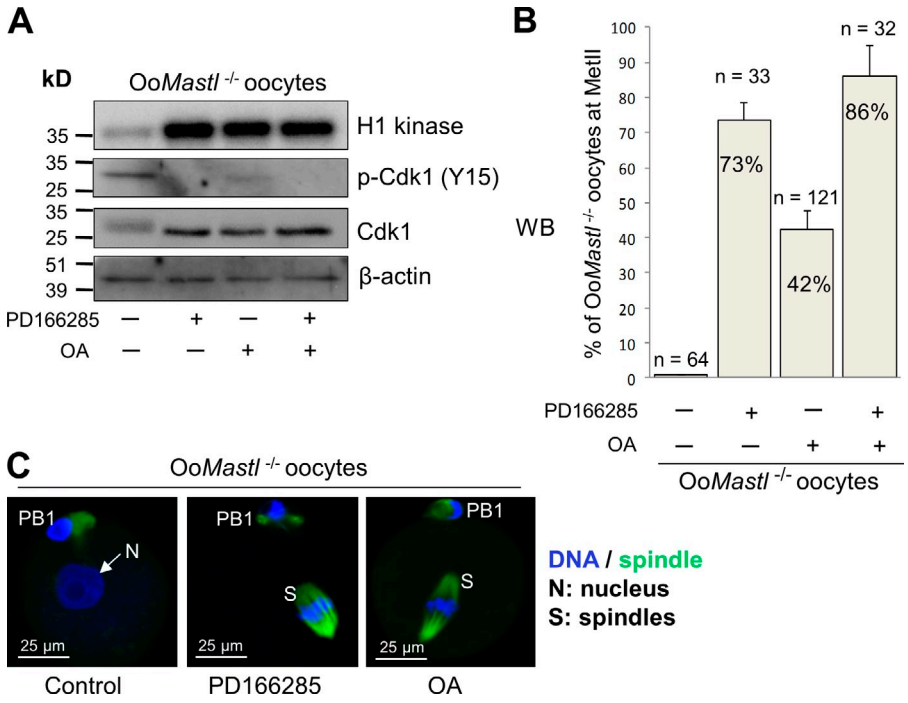

Figure 4. **Rescue of MII entry in Oo*Mastl*$^{-/-}$ oocytes upon Cdk1 activation and PP2A inhibition.** (A) Ovulated Oo*Mastl*$^{-/-}$ oocytes collected 16 h after hCG were treated with inhibitors that abolished the inhibitory phosphorylation on Cdk1 and enhanced Cdk1 activity in Oo*Mastl*$^{-/-}$ oocytes. Lysate from 50 oocytes was loaded in each lane, and β-actin was used as the loading control. (B) Rescue of MII entry in Oo*Mastl*$^{-/-}$ oocytes treated with PD166285 or OA. Error bars represent the SD. (C) Immunofluorescence of Oo*Mastl*$^{-/-}$ oocytes treated with inhibitors showing formation of spindles and chromosome condensation. All experiments were repeated at least three times, and representative results are shown.

To determine the reasons of the low Cdk1 activity in Oo*Mastl*$^{-/-}$ oocytes after PBE, we measured the levels of cyclin B1. In fact, the levels of cyclin B1 in Oo*Mastl*$^{-/-}$ oocytes were higher compared with Oo*Mastl*$^{+/+}$ oocytes (Fig. 3 D, ovulated oocytes), and this seems to be the result of low APC/C activity in Oo*Mastl*$^{-/-}$ oocytes (Fig. 1 E). However, the inhibitory phosphorylation of Cdk1 at Y15 was significantly increased in Oo*Mastl*$^{-/-}$ oocytes after PBE in both in vitro–cultured oocytes (Fig. 3 B, 14 h after GVBD) and in ovulated oocytes (Fig. 3 D). The increased inhibitory phosphorylation of Cdk1 in Oo*Mastl*$^{-/-}$ oocytes is most likely the reason for the low activity of Cdk1 after PBE (Fig. 3 A).

Collectively, our results indicate that *Mastl* depletion in mouse oocytes results in Cdk1 inactivation through its inhibitory phosphorylation at MII entry, but not during meiosis I. We propose that during MII entry, the suppression of PP2A activity by Mastl might prevent the dephosphorylation of Wee1B at its inhibitory sites and prevent the dephosphorylation of Cdc25B at its activating sites (Pal et al., 2008; Vigneron et al., 2009), both of which promote the activation of Cdk1.

To investigate whether the suppressed Cdk1 activity and failure of MII entry in Oo*Mastl*$^{-/-}$ oocytes resulted from elevated PP2A activity, we measured PP2A activity in oocytes immediately after PBE. We found that PP2A activity in Oo*Mastl*$^{+/+}$ oocytes was very low at this point, but PP2A activity in the Oo*Mastl*$^{-/-}$ oocytes was about nine times higher compared with Oo*Mastl*$^{+/+}$ oocytes (Fig. S3 B). These results indicate that the deletion of *Mastl* in mouse oocytes results in a dramatic elevation in PP2A activity specifically after the completion of meiosis I, and this prevents the entry into MII. Based on these findings, we suggest that Mastl-mediated suppression of PP2A plays an essential role in the rapid activation of Cdk1 and the phosphorylation of Cdk1 substrates required for MII entry. However, Mastl-mediated suppression of PP2A is not required for the entry and progression of meiosis I in mouse oocytes. At the moment, the identity of the specific PP2A isoform that is regulated by Mastl in mouse oocytes remains unclear because of the lack of specific antibodies against the B55 subunits. It would also be of interest to measure the PP2A activity using a known physiological substrate of Cdk1 during mouse oocyte maturation.

Cdk1 activation and PP2A inhibition drive Oo*Mastl*$^{-/-}$ oocytes into MII

We tested whether pharmacological activation of Cdk1 or inhibition of PP2A could lead to MII entry in Oo*Mastl*$^{-/-}$ oocytes. Treatment with the Wee1 inhibitor PD166285 (Li et al., 2002; Hashimoto et al., 2006) led to reduced levels of Cdk1 (Y15) phosphorylation and dramatically increased H1 kinase activity in Oo*Mastl*$^{-/-}$ oocytes (Fig. 4 A). This resulted in the breakdown of the nuclear membranes and chromosome condensation in all of the oocytes (n = 33), and 73% of the oocytes formed bipolar MII spindles (Fig. 4, B and C; and Fig. S3 E). Because PP2A activity is higher in Oo*Mastl*$^{-/-}$ oocytes after PBE (Fig. S3 B), we also treated the Oo*Mastl*$^{-/-}$ oocytes after PBE with the protein phosphatase inhibitor okadaic acid (OA; 50 nM; Cohen et al., 1989; Chang et al., 2011; Tay et al., 2012). Inhibition of phosphatases resulted in 42% (n = 121) of the Oo*Mastl*$^{-/-}$ oocytes forming bipolar spindles with aligned chromosomes (Fig. 4, B and C; and Fig. S3 E). Oocytes that failed to form MII spindles after culture with OA still contained nuclei (Fig. S3 E, OA). The OA treatment also led to an increase in Cdk1 activity and decreased Cdk1 phosphorylation on residue Y15 (Fig. 4 A). Finally, we found that the combination of both inhibitors led to the breakdown of the nuclear membrane in all the oocytes and had a moderate additive effect, with 86% of the Oo*Mastl*$^{-/-}$ oocytes forming bipolar spindles with aligned chromosomes (Fig. 4, B and C). This suggested that both Cdk1 and PP2A are involved in an interdependent manner during MII entry.

Published September 22, 2014

Ensa is absent in Oo*Mastl*$^{-/-}$ oocytes

We measured Ensa and Arpp19 protein levels in oocytes after PBE to investigate their involvement in the failure of Oo*Mastl*$^{-/-}$ oocytes to enter MII. Similar levels of Arpp19 were expressed in Oo*Mastl*$^{-/-}$ and Oo*Mastl*$^{+/+}$ oocytes, but the Ensa protein could not be detected in Oo*Mastl*$^{-/-}$ oocytes (Fig. 5 A and Fig. S3 C) despite comparable levels of *Ensa* mRNA (Fig. 5 B). We found that the Ensa protein levels were increased after GVBD in Oo*Mastl*$^{+/+}$ oocytes but Ensa was absent in Oo*Mastl*$^{-/-}$ oocytes (Fig. S3 C). A previous study in *Xenopus* egg extracts suggested that Mastl phosphorylates and activates Ensa, leading to PP2A inhibition (Mochida et al., 2010), but our data indicate the possibility that the translation or stability of Ensa is regulated by Mastl in mouse oocytes. We hypothesize that Mastl might be essential for the stability of Ensa through its phosphorylation.

Recent studies have shown that Mastl/Gwl kinase is essential for the initiation and progression of prometaphase during mitosis by suppressing the antagonizing activity of PP2A (Gharbi-Ayachi et al., 2010; Mochida et al., 2010; Domingo-Sananes et al., 2011; Mochida and Hunt, 2012; Álvarez-Fernández et al., 2013). In our study, however, we found that the *Mastl*-deficient oocytes entered meiosis I with normal timing and efficiency and progressed through prometaphase and metaphase I normally. These oocytes completed meiosis I with a delay in PBE as the result of insufficient APC/C activation. Moreover, we demonstrated that the *Mastl*-deficient oocytes failed to proceed to MII and instead entered interphase, which was caused by a failure to increase Cdk1 activity and was associated with an increase in PP2A activity.

Our results suggest that in mammalian oocytes Mastl activity is essential for entry into MII. In contrast, Mastl is not required for meiosis I entry but becomes important at the end of meiosis I for the activation of APC/C. Because PP2A has been shown to inhibit APC/C-dependent degradation of securin in HeLa cells (Hellmuth et al., 2014), it might be possible that increased PP2A activity in *Mastl*-null oocytes inhibits APC/C and delays the onset of anaphase I and PBE. Previous experiments have shown that the dual-specificity phosphatase Cdc14B negatively regulates the resumption and progression of meiosis in an APC/C-dependent manner (Schindler and Schultz, 2009). In the absence of Mastl, Cdc14B might act to counteract Cdk1 and thereby inhibit the transition from prophase to M phase.

The prometaphase of oocyte meiosis I is a lengthy process that takes around 6–8 h in mice (Polanski et al., 1998). This is in sharp contrast to the <30 min required for prometaphase in mitotic cells (Rieder et al., 1994). Our findings indicate that progression to metaphase I in mouse oocytes does not require Mastl-mediated PP2A suppression. Our data raise the possibility that the sustained PP2A activity causes the slow increase in Cdk1 activity and at the same time dephosphorylates Cdk1 substrates, which slows the progression of meiosis I.

In summary, Mastl is required in mouse oocytes for the timely activation of APC/C at the exit of meiosis I and is essential for the reactivation of Cdk1 needed for entry into MII. This study indicates a switch in the mechanisms that regulate Cdk1 activity between the two meiotic divisions in mouse oocytes and provides the starting point for a more detailed exploration of the mechanisms behind Mastl's role in mammalian meiosis.

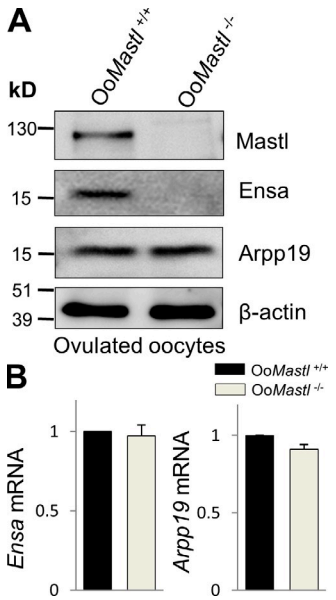

Figure 5. **Absence of Ensa protein expression in Oo*Mastl*$^{-/-}$ oocytes.** (A) Expression of Mastl, Ensa, and Arpp19 in ovulated Oo*Mastl*$^{+/+}$ and Oo*Mastl*$^{-/-}$ oocytes. Lysate from 100 oocytes was loaded in each lane. (B) Relative mRNA levels of *Ensa* and *Arpp19* in ovulated oocytes were determined by real-time PCR. The mRNA levels in the Oo*Mastl*$^{+/+}$ oocytes were set as 1.0, and the fold changes in Oo*Mastl*$^{-/-}$ oocytes are shown. Error bars represent SDs.

Materials and methods

Generation of *Mastl* conditional knockout mice

The *Mastl*^{FLOX} mouse strain was generated essentially as described previously for *Cdk1*^{FLOX} mice (Diril et al., 2012). Mouse genomic DNA harboring the *Mastl* locus was isolated from the BAC clone pBACe3.6 RP23-280K (Invitrogen). Using recombineering techniques (Lee et al., 2001), the *LoxP* recombination sites and a neomycin-selection cassette were introduced flanking the fourth coding exon of the mouse *Mastl* genomic locus. The 5′ homology arm comprised 3,690 bp (*Mus musculus* strain C57BL/6J GRCm38.p2 assembly, Chr2:23, 149, 361-23, 145, 671), whereas the 3′ homology arm included 5,899 bp (23, 138, 962-23, 144, 861). The resulting targeting vector (PKB926) was linearized by NotI digestion, and embryonic stem (ES) cells were electroporated. After positive and negative selection with Geneticin and ganciclovir, respectively, genomic DNA of surviving ES cell colonies was screened for homologous recombination by Southern hybridization using 5′ and 3′ probes (*M. musculus* strain C57BL/6J GRCm38.p2 assembly, Chr2:23, 153, 022-23, 150, 791 [PKO719/PKO720] and 23, 138, 362-23, 138, 961 [PKO756/PKO757]) located outside of the targeting vector. Correctly targeted ES cell clones (3002, 3003, 3004, and 3009) were identified and used for the generation of the Mastl conditional knockout mouse strain. To generate the *Mastl*^{FLOX} allele, the neomycin cassette was removed by crossing *Mastl* conditional knockout mice with *β-actin–Flpe* transgenic mice (Rodríguez et al., 2000; strain name: B6.Cg-Tg [ACTFLPe] 9205Dym/J; stock no. 005703; The Jackson Laboratory). *Mastl*$^{FLOX/FLOX}$ mice of a mixed background (129S1/SvImJ and C57BL/6) were backcrossed to C57BL/6J mice for four generations and crossed with transgenic mice carrying *Zp3* promoter–mediated Cre recombinase in a C57BL/6J background (de Vries et al., 2000). PCR genotyping primers sequences can be found in Table S1. After multiple rounds of crossing, we obtained homozygous mutant female mice lacking *Mastl* in their oocytes (Oo*Mastl*$^{-/-}$ mice). Littermates that did not carry the *Cre* transgene are referred to as Oo*Mastl*$^{+/+}$ mice and were used as controls.

All mice were housed under controlled environmental conditions with free access to water and food. Illumination was on between 6 am and 6 pm. Experimental protocols were approved by the regional ethical committee of the University of Gothenburg, Sweden, and by the Institutional Animal Care and Use Committee at the Biological Research Centre mouse facility at Biopolis, Singapore.

Published September 22, 2014

Reagents, antibodies, and immunological detection methods

Rabbit pAbs against Mastl were raised using an N-terminal 6-His–tagged peptide fragment from the mouse Mastl protein (residues 461–694, PKB908) as the antigen using a published protocol (Berthet et al., 2003). Rabbit pAbs against Arpp19 were raised using an N-terminal GST-tagged fusion protein of mouse Arpp19 (residues 25–112, PKB1506) as the antigen using a published protocol (Berthet et al., 2003). Mouse mAb against securin and rabbit pAb against Cdc20 were from Abcam. Human anti-CREST antibody was from Antibodies Inc., and rabbit anti-Mad2 antibody was obtained from Covance. Mouse mAbs against Cdk1 and HA were purchased from Santa-Cruz Biotechnology, Inc. Rabbit pAbs against Ensa, phospho-PP1α (Thr320), phospho–lamin A/C (Ser22), lamin A/C, cyclin B1, and phospho-Cdk1 (Y15) were obtained from Cell Signaling Technology. Mouse mAbs against β-actin, M2 and M16 media, dibutyryl-cAMP (dbcAMP), pregnant mare serum gonadotropin (PMSG), hCG, hyaluronidase, DAPI, mouse monoclonal anti–α-tubulin–FITC, and mineral oil were purchased from Sigma-Aldrich. OA and PD166285 were obtained from Tocris Bioscience. MK-1775 was obtained from Selleck Chemicals. Western blots were performed according to the instructions of the suppliers of the different antibodies and visualized using the ECL Prime Western Blotting Detection System (GE Healthcare). Alkaline phosphatase treatment was performed in 100 mM NaCl, 50 mM Tris-HCl, pH 7.9, 10 mM $MgCl_2$, and 1 mM DTT with the addition of 1 U rAPid alkaline phosphatase (Roche) for 1 h at 37°C.

β-Galactosidase staining of *Zp3-Cre; Rosa26 reporter* (*R26R*) ovaries

Zp3-Cre males were mated with *R26R* females (003474; The Jackson Laboratory) to generate the *Zp3-Cre; R26R* mice. Whole-mount β-galactosidase staining was performed to visualize the labeled oocytes in the postnatal day 10 (PD10) ovaries of *Zp3-Cre; R26R* mice. In brief, ovaries were fixed in 4% PFA for 1 h at 4°C and then rinsed three times for 15 min each in a buffer consisting of 1× PBS, pH 7.4, 2 mM magnesium chloride, 5 mM ethylene glycol tetraacetic acid, 0.01% sodium deoxycholate, and 0.02% NP-40 at RT. The ovaries were then incubated with a staining solution consisting of 1× PBS, pH 7.4, 2 mM magnesium chloride, 0.01% sodium deoxycholate, 0.02% NP-40, 5 mM potassium ferricyanide, 5 mM potassium ferrocyanide, and 1 mg/ml X-gal at 37°C overnight. After staining, the ovaries were refixed in 4% PFA for 8 h, embedded in paraffin, serially cut into 8-µm sections, and counterstained with 0.1% nuclear fast red solution. The sections were examined under an Axio Scope A1 upright microscope (Carl Zeiss).

Oocyte collection from gonadotropin-induced ovulation

To obtain ovulated oocytes for observation of PBE, immunostaining, and biochemical analysis, 3–4-wk-old female mice were injected intraperitoneally with 7.5 IU PMSG and 48 h later with 5 IU hCG. The ovulation usually occurred 12–14 h after the hCG injection (Hsieh et al., 2002). Ovulated oocytes were collected from the oviducts 16 h after hCG injection unless otherwise noted. Cumulus cells were removed by treatment with 0.3 mg/ml hyaluronidase in M2 medium. For Western blots, the oocytes were lysed in buffer containing 50 mM Tris-HCl, pH 8.0, 120 mM NaCl, 20 mM NaF, 20 mM β-glycerophosphate, 1 mM EDTA, 6 mM EGTA, pH 8.0, 1% NP-40, 1 mM DTT, 5 mM benzamidine, 1 mM PMSF, 250 µM sodium orthovanadate, 10 µg/ml aprotinin, 10 µg/ml leupeptin, and 1 µg/ml pepstatin.

Culture of ovulated oocytes with inhibitors

For inhibitor experiments, the protein phosphatase inhibitor OA (50 nM) and the Wee1 inhibitor PD166285 (10 µM) were added in M16 medium. Ovulated oocytes (those that contained a PB1 and a nucleus) collected 16 h after hCG treatment were treated for 6 h with PD166285, OA, or a combination of PD166285 and OA. When treated with OA, oocytes were treated for 10 h. For controls, oocytes were cultured with M16 medium.

GV-stage oocyte collection and culture

3–4-wk-old female mice were injected with 7.5 IU PMSG intraperitoneally, and 42–44 h later the mice were sacrificed and their ovaries were collected in 100 µg/ml dbcAMP-containing M2 medium. Fully grown GV-stage oocytes surrounded by cumulus cells were released by puncturing the ovaries in M2 medium supplemented with dbcAMP to maintain meiotic arrest during the in vitro operation. Oocytes were freed from the attached cumulus cells by repetitive pipetting through a narrow-bore glass pipette. When GV-stage oocytes were required for Western blots, the denuded oocytes were counted and lysed as described above. For immunofluorescence microscopy, GV-stage oocytes were fixed in PFA in PBS, pH 7.4, at RT.

To follow GVBD in vitro, the denuded oocytes were washed twice in dbcAMP-free M2 medium followed by a single washing in M16 medium. The oocytes were then cultured in M16 medium at 37°C in a humidified atmosphere of 5% CO_2 under mineral oil. 20 oocytes were cultured in a 50-µl drop of M16 medium. GVBD rates were recorded every 15 min after culturing in M16 medium.

To obtain GVBD oocytes for biochemical experiments, oocytes were collected 3 h after in vitro culture or at different time points of in vitro culture as mentioned in the respective figure legends. Oocytes were collected 3 h after GVBD for analysis at the prometaphase I stage and 6 h after GVBD for analysis at the metaphase I stage. The oocytes were lysed as described above.

Immunofluorescence and confocal microscopy

To determine the localization of Mastl protein in mouse oocytes, wild-type oocytes at GV, GVBD, and MetII stages were fixed in 4% PFA. After the fixed oocytes were permeabilized with 0.5% Triton X-100 at RT for 20 min, they were blocked with 1% BSA-supplemented PBS for 1 h and incubated at 4°C with Mastl antiserum overnight, followed by an incubation with Alexa Fluor 594 goat anti–rabbit IgG (Invitrogen) for 1 h at RT. Oo*Mastl*$^{-/-}$ oocytes were used as negative controls.

For spindle and DNA staining of oocytes at metaphase I, Oo*Mastl*$^{-/-}$ and Oo*Mastl*$^{+/+}$ oocytes that were cultured in M16 medium for 6 h after GVBD were fixed in 4% PFA at RT. For MetII spindle staining, ovulated oocytes harvested from the oviduct 16 h after hCG injection were fixed in 4% PFA. For assessing MII entry after inhibitor treatments, the cultured oocytes were fixed in 4% PFA at the end of their respective incubation periods. After the fixed oocytes were permeabilized with 0.5% Triton X-100 and blocked with 1% BSA-supplemented PBS as mentioned above, they were incubated with anti–α-tubulin–FITC antibody for 1 h at RT. After three washes in PBS containing 0.1% Tween 20 and 0.01% Triton X-100, the oocytes were costained with DAPI (1 µg/ml in PBS). Finally, the oocytes were mounted on glass slides with DABCO-containing mounting medium and examined by laser-scanning confocal microscopy (LSM 700; Carl Zeiss) with a Plan-Apochromat 20×/0.8 objective with the following band pass emission filters (in nm): 385–470 (DAPI), 505–530 (Alexa Fluor 488 and FITC), and 585–615 (Alexa Fluor 594). Z sections were analyzed and projected into one picture using the LSM image browser (Carl Zeiss). The images were then assembled by Illustrator CS2 (Adobe).

Fluorescence live imaging of oocyte maturation

Capped RNAs were synthesized in vitro with the T7 mMessage mMachine kit (Ambion) using linearized plasmids provided by M. Anger (Veterinary Research Institute in Brno, Brno, Czech Republic) and purified with the RNeasy Mini kit (QIAGEN). RNAs prepared at 150 ng/µl and 350 ng/µl for H2B-mCherry (for DNA visualization) and Map7-EGFP (for spindle visualization), respectively, were mixed in a 1:1 ratio and injected with an IM-6 (Narishige) into GV-stage oocytes placed in M2 medium supplemented with 0.2 mM 3-isobutyl-1-methylexanthine (IBMX; Sigma-Aldrich) at RT. Injected oocytes were cultured in M16 medium for 6 h in an incubator at 37°C and 5% CO_2. Time-lapse live epifluorescence imaging was performed with a DMI6000 B (Leica) equipped with an HCX PL FLUOTAR 20×/0.40 CORR objective, dichroic filters L5 and TX2, a heating stage at 37°C, and a stage cover maintaining 5% CO_2. Images were taken every 15 min for 16 h with an ORCA-ER charge-coupled device camera (Hamamatsu) operated by the MetaMorph software (Molecular Devices) and processed with ImageJ (National Institutes of Health).

Histone H1 kinase assay

Histone H1 kinase activity assays were performed using five oocytes in a 10-µl reaction volume based on a published protocol (Kudo et al., 2006). In brief, the reaction was performed in a buffer containing 25 mM HEPES, pH 7.4, 15 mM $MgCl_2$, 20 mM EGTA, 50 mM NaCl, 0.05% NP-40, 0.1 mM ATP, 100 mM PMSF, 1 mM DTT, 1 µg histone H1 (Roche), and 3 µCi γ-[^{32}P] ATP (PerkinElmer) and incubated at 37°C for 30 min. Samples were boiled in SDS sample buffer and then separated on a 15% SDS–polyacrylamide gel. The radioactive signal was detected by exposing the gels on an FLA 3000 phosphorimager (Fujifilm).

PP2A activity assay

PP2A activity was measured with the PP2A Immunoprecipitation Phosphatase Assay kit (EMD Millipore). In brief, PP2A was immunoprecipitated from lysates of oocytes (400 oocytes for each time point) in lysis buffer containing 20 mM imidazole-HCl, pH 7.0, 2 mM EDTA, 2 mM EGTA, 0.1% NP-40, and freshly added protease inhibitors (Roche). The PP2A protein was pulled down using anti-PP2A antibodies (clone 1D6; EMD Millipore)

Published September 22, 2014

and protein A agarose beads, after which it was incubated with the synthetic phosphopeptide K-R-pT-I-R-R at 30°C for 10 min before detection with malachite green phosphate detection solution (EMD Millipore) according to the manufacturer's instructions. The resulting color intensity was measured at 650 nm with a POLARstar Omega microplate reader (BMG LABTECH GmbH). Although this assay has been routinely used for measuring PP2A activity (Tay et al., 2012; Fan et al., 2013; Wei et al., 2013), it does not use a peptide substrate derived from a known physiological substrate of Cdk1 that is dephosphorylated by PP2A-B55. Previous experiments have used such a substrate in experiments with *Xenopus* egg extracts (Mochida et al., 2009, 2010), but such methods have not yet been optimized for use in mouse oocytes. Because the substrate specificity of PP2A is regulated by its associated B subunits, optimization of such a method for use with mouse oocytes would be able to characterize the activity of B55-associated PP2A in *Mastl*-null oocytes in future studies.

DNA replication analysis by BrdU incorporation

After GVBD, oocytes were allowed to mature for 14 h in M16 medium, and oocytes with PB1 were transferred to M16 medium containing 100 µM BrdU (Sigma-Aldrich) and allowed to mature for another 10 h. Oocytes were fixed in 4% PFA. After permeabilization with 0.5% Triton X-100 at RT for 20 min, oocytes were incubated in 4 M HCl solution at RT for 10 min. After neutralization for 10 min in 100 mM Tris-HCl, pH 8.0, and a second fixation with 4% PFA for 20 min at RT, oocytes were blocked overnight at 4°C with 1% BSA-supplemented PBS. Oocytes were labeled with BrdU mouse mAb (clone MoBU-1; 1:200 dilution) and Alexa Fluor 488 conjugate (Life Technologies) for 2 h at RT. After three washes in PBS containing 0.1% Tween 20 and 0.01% Triton X-100, the oocytes were costained with DAPI (1 µg/ml in PBS). Finally, the oocytes were mounted on glass slides with DABCO-containing mounting medium and examined by laser-scanning confocal microscopy (LSM 700 Inverted).

Real-time quantitative PCR

Total RNA was isolated from oocytes using the RNeasy Mini kit according to the manufacturer's instructions. Oligo (dT)–primed cDNA was synthesized using qScript reverse transcription (Quanta Biosciences). Real-time quantitative PCR for *Ensa* was performed using primers 5′-CCTGAGAAAGCTGAGGAGGC-3′ and 5′-AGGTTCTTGTCTGCTCCTGC-3′ and for *Arpp19* using primers 5′-CCGCAACCTTTGAGGGAAAG-3′ and 5′-CCTCCAGGCTTTTGTCCCAA-3′ on an ABI 7500 Real-Time PCR System (Applied Biosystems) using SYBR Green PCR master mix (Applied Biosystems). The reactions were performed in triplicate. Threshold cycle (Ct) values were obtained, and the ΔΔCt method was used to calculate the fold changes. All of the values were normalized to *Gapdh*.

Overexpression of HA-Ensa and HA-Arpp19 proteins in HEK293 cells

Mouse *Ensa* and *Arpp19* cDNAs were amplified by RT-PCR from RNA extracted from mouse embryonic fibroblasts. After the introduction of N-terminal HA tags by PCR, the cDNAs were cloned into pBOBI mammalian expression vectors and the sequences were verified. For expressing the Ensa and Arpp19 proteins, *pBOBI-HA-Ensa* (PKB1481) and *pBOBI-HA-Arpp19* (PKB1483) plasmids were transfected into HEK293 cells using Lipofectamine 2000 reagent (Invitrogen) according to the manufacturer's instructions. Cell lysates were prepared in EBN buffer (80 mM β-glycerophosphate, pH 7.3, 20 mM EGTA, 15 mM $MgCl_2$, 150 mM NaCl, 0.5% NP-40, 1 mM DTT, and protease inhibitors [20 µg/ml each of leupeptin, chymostatin, and pepstatin; EI8, EI6, and EI10; EMD Millipore]) for 20 min with constant shaking at 1,200 rpm. Lysates were centrifuged for 30 min at 18,000 *g* at 4°C, and supernatants were snap-frozen in liquid nitrogen and stored at −80°C.

Statistical analysis

All experiments were repeated at least three times. For comparisons between groups, the differences were calculated with Student's *t* test, and a difference was considered to be significant if $P < 0.05$.

Online supplemental material

Fig. S1 shows the phosphorylation and localization of Mastl in mouse oocytes and generation of *Mastl* conditional knockout mice. Fig. S2 shows that although the *Mastl* conditional knockout females are infertile, the spindle, chromosome condensation, and SAC activation in the oocyte are normal and *Mastl*-null oocytes enter S phase after PBE. Fig. S3 shows the PP2A activities and Ensa protein levels during oocyte maturation. Table S1 lists PCR genotyping primers. Video 1 shows the normal MII entry in an Oo*Mastl*$^{+/+}$ oocyte. Video 2 shows the failure of MII entry in an Oo*Mastl*$^{-/-}$ oocyte by live imaging. Online supplemental material is available at http://www.jcb.org/cgi/content/full/jcb.201406033/DC1.

We are thankful to Eileen Southon and Susan Reid (National Cancer Institute–Frederick, Frederick, MD) for help in generating the *Mastl*$^{FLOX/FLOX}$ mice and to the staff at the University of Gothenburg core facility for cellular imaging for assistance with confocal microscopy.

This study was supported by grants (to K. Liu) from the Jane and Dan Olssons Foundation, the LUA/ALF-medel Västra Götalandsregionen, AFA Insurance, the Swedish Research Council, and the Swedish Cancer Foundation; by funding (to P. Kaldis) from the Biomedical Research Council of A*STAR, Singapore; and by funding (to N.R. Kudo) from the Medical Research Council and the Genesis Research Trust.

The authors declare no competing financial interests.

Submitted: 9 June 2014
Accepted: 25 August 2014

References

Álvarez-Fernández, M., R. Sánchez-Martínez, B. Sanz-Castillo, P.P. Gan, M. Sanz-Flores, M. Trakala, M. Ruiz-Torres, T. Lorca, A. Castro, and M. Malumbres. 2013. Greatwall is essential to prevent mitotic collapse after nuclear envelope breakdown in mammals. *Proc. Natl. Acad. Sci. USA*. 110:17374–17379. http://dx.doi.org/10.1073/pnas.1310745110

Archambault, V., X. Zhao, H. White-Cooper, A.T. Carpenter, and D.M. Glover. 2007. Mutations in *Drosophila* Greatwall/Scant reveal its roles in mitosis and meiosis and interdependence with Polo kinase. *PLoS Genet.* 3:e200. http://dx.doi.org/10.1371/journal.pgen.0030200

Berthet, C., E. Aleem, V. Coppola, L. Tessarollo, and P. Kaldis. 2003. Cdk2 knockout mice are viable. *Curr. Biol.* 13:1775–1785. http://dx.doi.org/10.1016/j.cub.2003.09.024

Burgess, A., S. Vigneron, E. Brioudes, J.C. Labbé, T. Lorca, and A. Castro. 2010. Loss of human Greatwall results in G2 arrest and multiple mitotic defects due to deregulation of the cyclin B-Cdc2/PP2A balance. *Proc. Natl. Acad. Sci. USA*. 107:12564–12569. http://dx.doi.org/10.1073/pnas.0914191107

Chang, H.Y., P.C. Jennings, J. Stewart, N.M. Verrills, and K.T. Jones. 2011. Essential role of protein phosphatase 2A in metaphase II arrest and activation of mouse eggs shown by okadaic acid, dominant negative protein phosphatase 2A, and FTY720. *J. Biol. Chem.* 286:14705–14712. http://dx.doi.org/10.1074/jbc.M110.193227

Cohen, P., S. Klumpp, and D.L. Schelling. 1989. An improved procedure for identifying and quantitating protein phosphatases in mammalian tissues. *FEBS Lett.* 250:596–600. http://dx.doi.org/10.1016/0014-5793(89)80803-8

Cundell, M.J., R.N. Bastos, T. Zhang, J. Holder, U. Gruneberg, B. Novak, and F.A. Barr. 2013. The BEG (PP2A-B55/ENSA/Greatwall) pathway ensures cytokinesis follows chromosome separation. *Mol. Cell.* 52:393–405. http://dx.doi.org/10.1016/j.molcel.2013.09.005

Davydenko, O., R.M. Schultz, and M.A. Lampson. 2013. Increased CDK1 activity determines the timing of kinetochore-microtubule attachments in meiosis I. *J. Cell Biol.* 202:221–229. http://dx.doi.org/10.1083/jcb.201303019

de Vries, W.N., L.T. Binns, K.S. Fancher, J. Dean, R. Moore, R. Kemler, and B.B. Knowles. 2000. Expression of Cre recombinase in mouse oocytes: a means to study maternal effect genes. *Genesis*. 26:110–112. http://dx.doi.org/10.1002/(SICI)1526-968X(200002)26:2<110::AID-GENE2>3.0.CO;2-8

Diril, M.K., C.K. Ratnacaram, V.C. Padmakumar, T. Du, M. Wasser, V. Coppola, L. Tessarollo, and P. Kaldis. 2012. Cyclin-dependent kinase 1 (Cdk1) is essential for cell division and suppression of DNA re-replication but not for liver regeneration. *Proc. Natl. Acad. Sci. USA*. 109:3826–3831. http://dx.doi.org/10.1073/pnas.1115201109

Domingo-Sananes, M.R., O. Kapuy, T. Hunt, and B. Novak. 2011. Switches and latches: a biochemical tug-of-war between the kinases and phosphatases that control mitosis. *Philos. Trans. R. Soc. Lond. B Biol. Sci.* 366:3584–3594. http://dx.doi.org/10.1098/rstb.2011.0087

Dupré, A., E. Buffin, C. Roustan, A.C. Nairn, C. Jessus, and O. Haccard. 2013. The phosphorylation of ARPP19 by Greatwall renders the auto-amplification of MPF independently of PKA in *Xenopus* oocytes. *J. Cell Sci.* 126:3916–3926. http://dx.doi.org/10.1242/jcs.126599

Dupré, A., E.M. Daldello, A.C. Nairn, C. Jessus, and O. Haccard. 2014. Phosphorylation of ARPP19 by protein kinase A prevents meiosis resumption in *Xenopus* oocytes. *Nat. Commun.* 5:3318. http://dx.doi.org/10.1038/ncomms4318

Eppig, J.J., M.M. Viveiros, C.M. Bivens, and R. De La Fuente. 2004. Regulation of mammalian oocyte maturation. *In* The Ovary. Second edition. P.C.K. Leung, and E.Y. Adashi, editors. Elsevier Academic Press, San Diego. 113–129.

Fan, S., Q. Meng, J. Xu, Y. Jiao, L. Zhao, X. Zhang, F.H. Sarkar, M.L. Brown, A. Dritschilo, and E.M. Rosen. 2013. DIM (3,3′-diindolylmethane) confers protection against ionizing radiation by a unique mechanism. *Proc. Natl. Acad. Sci. USA*. 110:18650–18655. http://dx.doi.org/10.1073/pnas.1308206110

Gharbi-Ayachi, A., J.C. Labbé, A. Burgess, S. Vigneron, J.M. Strub, E. Brioudes, A. Van-Dorsselaer, A. Castro, and T. Lorca. 2010. The substrate of Greatwall kinase, Arpp19, controls mitosis by inhibiting protein phosphatase 2A. *Science*. 330:1673–1677. http://dx.doi.org/10.1126/science.1197048

Glover, D.M. 2012. The overlooked greatwall: a new perspective on mitotic control. *Open Biol.* 2:120023. http://dx.doi.org/10.1098/rsob.120023

Haas, M., and E. Jost. 1993. Functional analysis of phosphorylation sites in human lamin A controlling lamin disassembly, nuclear transport and assembly. *Eur. J. Cell Biol.* 62:237–247.

Hashimoto, O., M. Shinkawa, T. Torimura, T. Nakamura, K. Selvendiran, M. Sakamoto, H. Koga, T. Ueno, and M. Sata. 2006. Cell cycle regulation by the Wee1 inhibitor PD0166285, pyrido [2,3-d] pyimidine, in the B16 mouse melanoma cell line. *BMC Cancer*. 6:292. http://dx.doi.org/10.1186/1471-2407-6-292

Hellmuth, S., F. Böttger, C. Pan, M. Mann, and O. Stemmann. 2014. PP2A delays APC/C-dependent degradation of separase-associated but not free securin. *EMBO J.* 33:1134–1147. http://dx.doi.org/10.1002/embj.201488098

Hsieh, M., M.A. Johnson, N.M. Greenberg, and J.S. Richards. 2002. Regulated expression of Wnts and Frizzleds at specific stages of follicular development in the rodent ovary. *Endocrinology*. 143:898–908. http://dx.doi.org/10.1210/endo.143.3.8684

Jin, F., M. Hamada, L. Malureanu, K.B. Jeganathan, W. Zhou, D.E. Morbeck, and J.M. van Deursen. 2010. Cdc20 is critical for meiosis I and fertility of female mice. *PLoS Genet.* 6:e1001147. http://dx.doi.org/10.1371/journal.pgen.1001147

Jones, K.T. 2004. Turning it on and off: M-phase promoting factor during meiotic maturation and fertilization. *Mol. Hum. Reprod.* 10:1–5. http://dx.doi.org/10.1093/molehr/gah009

Kim, M.Y., E. Bucciarelli, D.G. Morton, B.C. Williams, K. Blake-Hodek, C. Pellacani, J.R. Von Stetina, X. Hu, M.P. Somma, D. Drummond-Barbosa, and M.L. Goldberg. 2012. Bypassing the Greatwall-Endosulfine pathway: plasticity of a pivotal cell-cycle regulatory module in *Drosophila melanogaster* and *Caenorhabditis elegans*. *Genetics*. 191:1181–1197. http://dx.doi.org/10.1534/genetics.112.140574

Kitajima, T.S., M. Ohsugi, and J. Ellenberg. 2011. Complete kinetochore tracking reveals error-prone homologous chromosome biorientation in mammalian oocytes. *Cell*. 146:568–581. http://dx.doi.org/10.1016/j.cell.2011.07.031

Kubiak, J.Z., M. Weber, G. Géraud, and B. Maro. 1992. Cell cycle modification during the transitions between meiotic M-phases in mouse oocytes. *J. Cell Sci.* 102:457–467.

Kudo, N.R., K. Wassmann, M. Anger, M. Schuh, K.G. Wirth, H. Xu, W. Helmhart, H. Kudo, M. McKay, B. Maro, et al. 2006. Resolution of chiasmata in oocytes requires separase-mediated proteolysis. *Cell*. 126:135–146. http://dx.doi.org/10.1016/j.cell.2006.05.033

Lee, E.C., D. Yu, J. Martinez de Velasco, L. Tessarollo, D.A. Swing, D.L. Court, N.A. Jenkins, and N.G. Copeland. 2001. A highly efficient *Escherichia coli*-based chromosome engineering system adapted for recombinogenic targeting and subcloning of BAC DNA. *Genomics*. 73:56–65. http://dx.doi.org/10.1006/geno.2000.6451

Li, J., Y. Wang, Y. Sun, and T.S. Lawrence. 2002. Wild-type TP53 inhibits G_2-phase checkpoint abrogation and radiosensitization induced by PD0166285, a WEE1 kinase inhibitor. *Radiat. Res.* 157:322–330. http://dx.doi.org/10.1667/0033-7587(2002)157[0322:WTTIGP]2.0.CO;2

Li, Y.H., H. Kang, Y.N. Xu, Y.T. Heo, X.S. Cui, N.H. Kim, and J.S. Oh. 2013. Greatwall kinase is required for meiotic maturation in porcine oocytes. *Biol. Reprod.* 89:53. http://dx.doi.org/10.1095/biolreprod.113.109850

Lorca, T., and A. Castro. 2012. Deciphering the new role of the Greatwall/PP2A pathway in cell cycle control. *Genes Cancer*. 3:712–720. http://dx.doi.org/10.1177/1947601912473478

Madgwick, S., D.V. Hansen, M. Levasseur, P.K. Jackson, and K.T. Jones. 2006. Mouse Emi2 is required to enter meiosis II by reestablishing cyclin B1 during interkinesis. *J. Cell Biol.* 174:791–801. http://dx.doi.org/10.1083/jcb.200604140

McGuinness, B.E., M. Anger, A. Kouznetsova, A.M. Gil-Bernabé, W. Helmhart, N.R. Kudo, A. Wuensche, S. Taylor, C. Hoog, B. Novak, and K. Nasmyth. 2009. Regulation of APC/C activity in oocytes by a Bub1-dependent spindle assembly checkpoint. *Curr. Biol.* 19:369–380. http://dx.doi.org/10.1016/j.cub.2009.01.064

Mochida, S., and T. Hunt. 2012. Protein phosphatases and their regulation in the control of mitosis. *EMBO Rep.* 13:197–203. http://dx.doi.org/10.1038/embor.2011.263

Mochida, S., S. Ikeo, J. Gannon, and T. Hunt. 2009. Regulated activity of PP2A-B55 delta is crucial for controlling entry into and exit from mitosis in *Xenopus* egg extracts. *EMBO J.* 28:2777–2785. http://dx.doi.org/10.1038/emboj.2009.238

Mochida, S., S.L. Maslen, M. Skehel, and T. Hunt. 2010. Greatwall phosphorylates an inhibitor of protein phosphatase 2A that is essential for mitosis. *Science*. 330:1670–1673. http://dx.doi.org/10.1126/science.1195689

Nabti, I., P. Marangos, J. Bormann, N.R. Kudo, and J. Carroll. 2014. Dual-mode regulation of the APC/C by CDK1 and MAPK controls meiosis I progression and fidelity. *J. Cell Biol.* 204:891–900. http://dx.doi.org/10.1083/jcb.201305049

Okumura, E., A. Morita, M. Wakai, S. Mochida, M. Hara, and T. Kishimoto. 2014. Cyclin B-Cdk1 inhibits protein phosphatase PP2A-B55 via a Greatwall kinase-independent mechanism. *J. Cell Biol.* 204:881–889. http://dx.doi.org/10.1083/jcb.201307160

Pal, G., M.T.Z. Paraz, and D.R. Kellogg. 2008. Regulation of Mih1/Cdc25 by protein phosphatase 2A and casein kinase 1. *J. Cell Biol.* 180:931–945. http://dx.doi.org/10.1083/jcb.200711014

Pesin, J.A., and T.L. Orr-Weaver. 2008. Regulation of APC/C activators in mitosis and meiosis. *Annu. Rev. Cell Dev. Biol.* 24:475–499. http://dx.doi.org/10.1146/annurev.cellbio.041408.115949

Peter, M., J. Nakagawa, M. Dorée, J.C. Labbé, and E.A. Nigg. 1990. In vitro disassembly of the nuclear lamina and M phase-specific phosphorylation of lamins by cdc2 kinase. *Cell*. 61:591–602. http://dx.doi.org/10.1016/0092-8674(90)90471-P

Polanski, Z., E. Ledan, S. Brunet, S. Louvet, M.H. Verlhac, J.Z. Kubiak, and B. Maro. 1998. Cyclin synthesis controls the progression of meiotic maturation in mouse oocytes. *Development*. 125:4989–4997.

Rangone, H., E. Wegel, M.K. Gatt, E. Yeung, A. Flowers, J. Debski, M. Dadlez, V. Janssens, A.T. Carpenter, and D.M. Glover. 2011. Suppression of scant identifies Endos as a substrate of greatwall kinase and a negative regulator of protein phosphatase 2A in mitosis. *PLoS Genet.* 7:e1002225. http://dx.doi.org/10.1371/journal.pgen.1002225

Rieder, C.L., A. Schultz, R. Cole, and G. Sluder. 1994. Anaphase onset in vertebrate somatic cells is controlled by a checkpoint that monitors sister kinetochore attachment to the spindle. *J. Cell Biol.* 127:1301–1310. http://dx.doi.org/10.1083/jcb.127.5.1301

Rodríguez, C.I., F. Buchholz, J. Galloway, R. Sequerra, J. Kasper, R. Ayala, A.F. Stewart, and S.M. Dymecki. 2000. High-efficiency deleter mice show that FLPe is an alternative to Cre-loxP. *Nat. Genet.* 25:139–140. http://dx.doi.org/10.1038/75973

Schindler, K., and R.M. Schultz. 2009. CDC14B acts through FZR1 (CDH1) to prevent meiotic maturation of mouse oocytes. *Biol. Reprod.* 80:795–803. http://dx.doi.org/10.1095/biolreprod.108.074906

Tay, K.H., L. Jin, H.Y. Tseng, C.C. Jiang, Y. Ye, R.F. Thorne, T. Liu, S.T. Guo, N.M. Verrills, P. Hersey, and X.D. Zhang. 2012. Suppression of PP2A is critical for protection of melanoma cells upon endoplasmic reticulum stress. *Cell Death Dis.* 3:e337. http://dx.doi.org/10.1038/cddis.2012.79

Vigneron, S., E. Brioudes, A. Burgess, J.C. Labbé, T. Lorca, and A. Castro. 2009. Greatwall maintains mitosis through regulation of PP2A. *EMBO J.* 28:2786–2793. http://dx.doi.org/10.1038/emboj.2009.228

Virshup, D.M., and P. Kaldis. 2010. Cell biology. Enforcing the Greatwall in mitosis. *Science*. 330:1638–1639. http://dx.doi.org/10.1126/science.1199898

Voets, E., and R.M. Wolthuis. 2010. MASTL is the human orthologue of Greatwall kinase that facilitates mitotic entry, anaphase and cytokinesis. *Cell Cycle*. 9:3591–3601. http://dx.doi.org/10.4161/cc.9.17.12832

Von Stetina, J.R., S. Tranguch, S.K. Dey, L.A. Lee, B. Cha, and D. Drummond-Barbosa. 2008. α-Endosulfine is a conserved protein required for oocyte meiotic maturation in *Drosophila*. *Development*. 135:3697–3706. http://dx.doi.org/10.1242/dev.025114

Wang, P., X. Pinson, and V. Archambault. 2011. PP2A-twins is antagonized by greatwall and collaborates with polo for cell cycle progression and centrosome attachment to nuclei in *Drosophila* embryos. *PLoS Genet.* 7:e1002227. http://dx.doi.org/10.1371/journal.pgen.1002227

Wang, P., J.A. Galan, K. Normandin, É. Bonneil, G.R. Hickson, P.P. Roux, P. Thibault, and V. Archambault. 2013. Cell cycle regulation of Greatwall kinase nuclear localization facilitates mitotic progression. *J. Cell Biol.* 202:277–293. http://dx.doi.org/10.1083/jcb.201211141

Wassmann, K., T. Niault, and B. Maro. 2003. Metaphase I arrest upon activation of the Mad2-dependent spindle checkpoint in mouse oocytes. *Curr. Biol.* 13:1596–1608. http://dx.doi.org/10.1016/j.cub.2003.08.052

Wei, D., L.A. Parsels, D. Karnak, M.A. Davis, J.D. Parsels, A.C. Marsh, L. Zhao, J. Maybaum, T.S. Lawrence, Y. Sun, and M.A. Morgan. 2013. Inhibition of protein phosphatase 2A radiosensitizes pancreatic can-

cers by modulating CDC25C/CDK1 and homologous recombination repair. *Clin. Cancer Res.* 19:4422–4432. http://dx.doi.org/10.1158/1078-0432.CCR-13-0788

Yu, J., S.L. Fleming, B. Williams, E.V. Williams, Z. Li, P. Somma, C.L. Rieder, and M.L. Goldberg. 2004. Greatwall kinase: a nuclear protein required for proper chromosome condensation and mitotic progression in *Drosophila*. *J. Cell Biol.* 164:487–492. http://dx.doi.org/10.1083/jcb.200310059

Yu, J., Y. Zhao, Z. Li, S. Galas, and M.L. Goldberg. 2006. Greatwall kinase participates in the Cdc2 autoregulatory loop in *Xenopus* egg extracts. *Mol. Cell*. 22:83–91. http://dx.doi.org/10.1016/j.molcel.2006.02.022

Adhikari et al., http://www.jcb.org/cgi/content/full/jcb.201406033/DC1

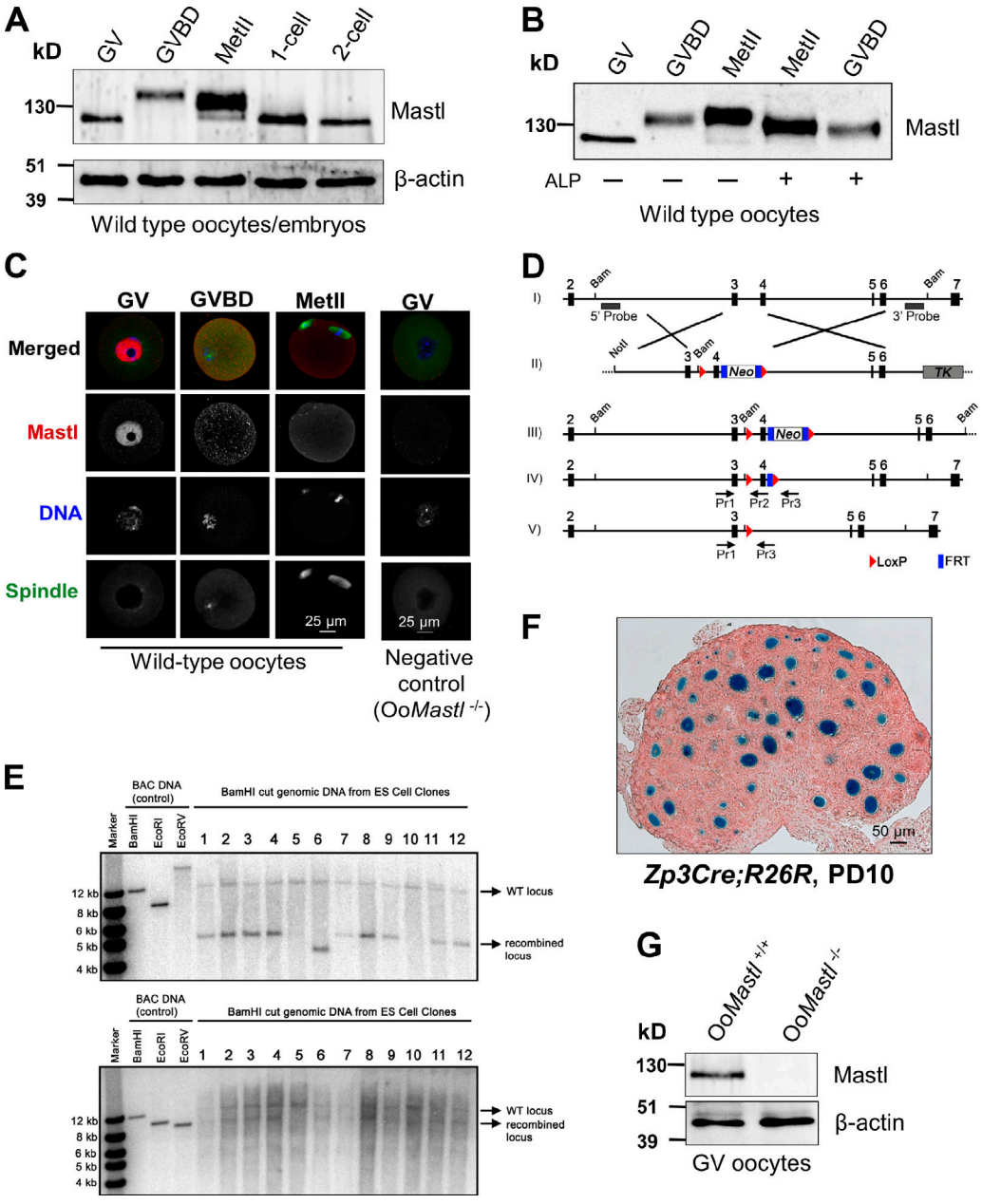

Figure S1. **Phosphorylation and localization of Mastl in mouse oocytes and generation of *Mastl* conditional knockout mice.** (A) Immunoblotting for Mastl during oocyte maturation and in early embryos. (B) Mobility shift of Mastl after the treatment of wild-type oocyte lysates with alkaline phosphatase (ALP). (C) Mastl was localized in the GV before meiotic resumption but was found throughout the ooplasm of the oocytes at the GVBD and MetII stages. Oo*Mastl*$^{-/-}$ oocytes were used as negative controls. 30 oocytes per group were analyzed, and representative images are shown. (D) The murine *Mastl* genomic locus (I) was modified in ES cells with the targeting vector (II). An FRT-flanked (blue rectangles) neomycin-selection cassette was introduced along with two *LoxP* recombination sites (red triangles) on both sides of exon 4, and this generated a mutant *Mastl* locus (III). For Southern blot analysis, 5′ and 3′ probes located outside of the targeting vector were used as above. BamHI digestion yields a 12.5-kb fragment in the wild-type locus and a 5.1-kb (detectable by the 5′ probe) and 9.1-kb (detectable by the 3′ probe) fragment in the homologous recombined locus. Upon expression of FLP recombinase, the neomycin cassette is removed and only the *LoxP* sites flanking exon 4 remain in the locus (IV, *Mastl*^{FLOX}). Cre recombinase expression leads to excision of exon 4 (V), and this results in total deletion of the *Mastl* gene product caused by a frame shift. PCR genotyping primers are indicated (Pr1, Pr2, and Pr3), and the sequences can be found in Table S1. (E) Genomic DNA isolated from double-selected ES cell colonies was digested with BamHI and analyzed by Southern hybridization using a 5′ probe (PKO721/PKO722, 500 bp). Homologous recombination at the 5′ site yields a 5.1-kb fragment (top). Genomic DNA was analyzed as above using a 3′ probe (PKO756/757, 600 bp). Homologous recombination at the 3′ site yields a 9.1-kb fragment. One of the ES cell clones (clone 3) that had undergone homologous recombination at both the 5′ and 3′ sites of exon 4 was selected for generation of the chimera (bottom). (F) β-Galactosidase staining (blue) in oocytes showing the high efficiency and specificity of the *Zp3-Cre* mouse line. (G) Oocyte-specific deletion of Mastl. For A, B, and G, lysate from 100 oocytes or embryos was loaded in each lane. The levels of β-actin were used as the control.

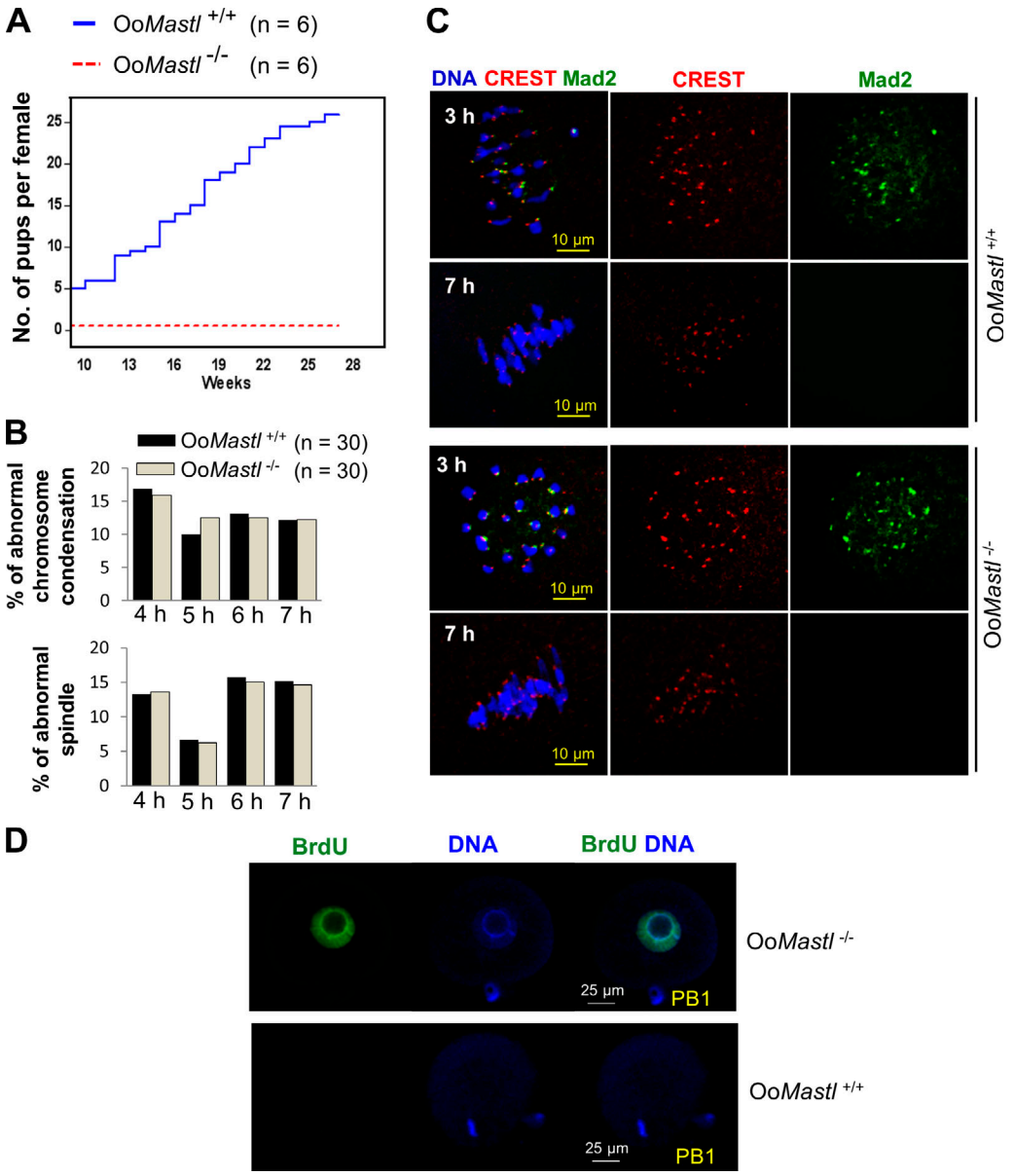

Figure S2. **Infertility of *Mastl* conditional knockout females, normal spindle and chromosome condensation, Mad2 dissociation from kinetochores, and BrdU incorporation in oocytes.** (A) Comparison of the cumulative number of pups per Oo*Mastl*$^{-/-}$ female (red dotted line) and per Oo*Mastl*$^{+/+}$ female (blue line). All Oo*Mastl*$^{-/-}$ females were infertile. Number of females monitored (n) is shown. (B) Comparison of the percentages of oocytes with abnormal spindle formation and abnormal chromosome condensation. Oocytes were cultured in vitro for the indicated periods after GVBD before staining for chromosomes, spindles, and kinetochores. (C) Representative images of immunostaining for DNA, CREST, and Mad2. Oocytes were fixed for immunostaining at either 3 or 7 h after GVBD. 30 oocytes were analyzed for each time point. (D) BrdU incorporation into decondensed chromatin of Oo*Mastl*$^{-/-}$ oocytes after PBE. The experiment was conducted three times using at least 10 oocytes per group, and representative images are shown.

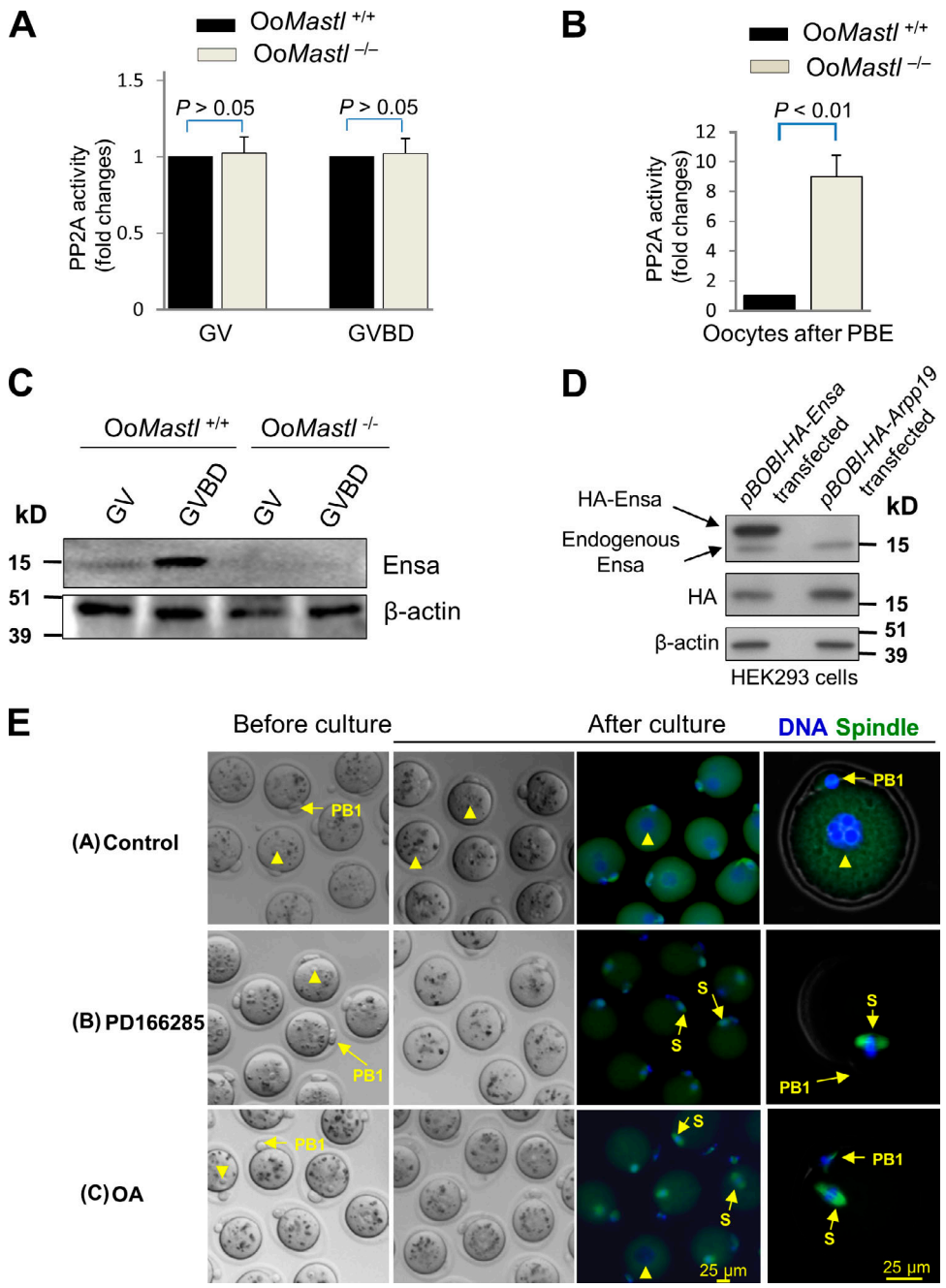

Figure S3. **PP2A activities and Ensa protein levels during oocyte maturation.** (A) Comparable PP2A activities in meiosis I in Oo*Mastl*$^{-/-}$ and Oo*Mastl*$^{+/+}$ oocytes. (B) Significantly elevated PP2A activity in Oo*Mastl*$^{-/-}$ oocytes after PBE ($P < 0.01$). For A and B, lysate from 400 oocytes was used for each time point, and error bars represent SD. The PP2A activity in the Oo*Mastl*$^{+/+}$ oocytes was set as 1.0, and fold changes in Oo*Mastl*$^{-/-}$ oocytes are shown. All experiments were repeated at least three times. The activity of PP2A immunoprecipitated by anti-PP2A antibody (specific to the catalytic subunit of PP2A) was related to the amount of inorganic phosphate released by dephosphorylating the phosphopeptide K-R-pT-I-R-R. (C) Expression of Ensa in GV and GVBD oocytes. (D) Validation of the specificity of the Ensa antibody (#8770; Cell Signaling Technology). The antibody specifically detects overexpressed HA-Ensa protein but does not cross-react with the HA-Arpp19 protein. As a control, anti-HA antibodies detect both the HA-Ensa and HA-Arpp19 proteins in the transfected HEK293 cells. The levels of β-actin were used as a loading control. In each lane, 10 μg cell lysate was loaded, and representative results of three repeated experiments are shown. (E) A representative experiment for obtaining data for Fig. 4. Before treatment with inhibitors, all of the oocytes contained a nucleus (arrowheads) and a PB1. Immunofluorescence of Oo*Mastl*$^{-/-}$ oocytes treated with inhibitors indicating formation of spindles (S) and chromosome condensation. All experiments were repeated at least three times, and representative results are shown.

Table S1. **PCR genotyping primers**

Primer name	Primer sequence
5′ Probe Forward, PKO721	5′-TTGGTGATTATATTGTTAATGAAACTG-3′
5′ Probe Reverse, PKO722	5′-AAAAAAGGATTACGGATTACAAAGCTTC-3′
3′ Probe Forward, PKO756	5′-CCTAGTTGTAAAACGTAATGCTTA-3′
3′ Probe Reverse, PKO757	5′-AGGGATCCCTGTCCCTATCTTTA-3′
Genotyping Pr1, PKO860	5′-CATGCCTTCCTTGAAAGAGGTGGAC-3′
Genotyping Pr2, PKO862	5′-GTGGGAGGAATTACAAGAGACAAC-3′
Genotyping Pr3, PKO863	5′-GGCAGGTGGAGGCAAGAGCTCACAGA-3′

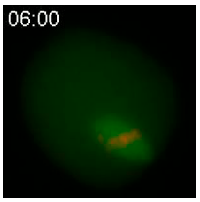

Video 1. **Live imaging showing the normal MII entry in Oo*Mastl*$^{+/+}$ oocytes.** Oo*Mastl*$^{+/+}$ oocytes at the GV stage were microinjected with mRNAs to allow the expression of H2B-mCherry (red fluorescence for labeling DNA) and Map7-EGFP (green fluorescence for labeling spindle microtubules). The oocytes were cultured for 6 h after GVBD when the oocytes reached the metaphase I stage. Images were analyzed by epifluorescence live cell time-lapse microscopy using a DMI6000 B microscope equipped with an HCX PL FLUOTAR 20×/0.40 CORR objective, dichroic filters L5 and TX2, a heating stage at 37°C, and a stage cover maintaining 5% CO_2. Images were taken every 15 min for 16 h with an ORCA-ER charge-coupled device camera operated by MetaMorph software. In seven independent experiments, a total of 30 Oo*Mastl*$^{+/+}$ oocytes were analyzed. In this particular experiment, Oo*Mastl*$^{+/+}$ oocytes established metaphase I (07:15), extruded the PB1 (anaphase I), subsequently reformed bipolar spindles (prometaphase II), and aligned chromosomes again (MetII).

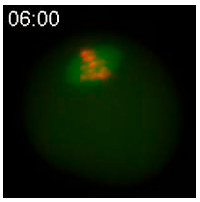

Video 2. **Live imaging showing the failure of MII entry in Oo*Mastl*$^{-/-}$ oocytes.** Oo*Mastl*$^{-/-}$ oocytes at the GV stage were microinjected with mRNAs to allow the expression of H2B-mCherry (red fluorescence for labeling DNA) and Map7-EGFP (green fluorescence for labeling spindle microtubules). The oocytes were cultured for 6 h after GVBD when the oocytes reached the metaphase I stage. Images were analyzed by epifluorescence live cell time-lapse microscopy using a DMI6000 B microscope equipped with an HCX PL FLUOTAR 20×/0.40 CORR objective, dichroic filters L5 and TX2, a heating stage at 37°C, and a stage cover maintaining 5% CO_2. Images were taken every 15 min for 16 h with an ORCA-ER charge-coupled device camera operated by MetaMorph software. In seven independent experiments, a total of 14 Oo*Mastl*$^{-/-}$ oocytes were analyzed. The Oo*Mastl*$^{-/-}$ oocytes also established metaphase I (07:15), but upon completion of chromosome segregation, the chromosomes were decondensed, leading to nucleus reformation. Chromosomes were not recondensed and microtubules did not reform bipolar spindles during the observation period, suggesting that completion of meiosis I was followed by an interphase without any observable indication of MII in Oo*Mastl*$^{-/-}$ oocytes.